Probing molecule-surface interactions through ultra-fast adsorbate dynamics: propane/Pt(111)

2008 New J. Phys. 10 125026

(http://iopscience.iop.org/1367-2630/10/12/125026)

New Journal of Physics
The open-access journal for physics

Probing molecule–surface interactions through ultra-fast adsorbate dynamics: propane/Pt(111)

A P Jardine, H Hedgeland, D Ward, Y Xiaoqing[1], W Allison, J Ellis and G Alexandrowicz[2]

Cavendish Laboratory, University of Cambridge, JJ Thomson Avenue, Cambridge CB3 0HE, UK
E-mail: ga232@cam.ac.uk

New Journal of Physics **10** (2008) 125026 (20pp)
Received 31 March 2008
Published 22 December 2008
Online at http://www.njp.org/
doi:10.1088/1367-2630/10/12/125026

Abstract. ^{3}He spin echo measurements of the atomic scale motion of propane on a Pt(111) surface are presented. The measurements provide both the height of the energy barriers to diffusion and the strength of the frictional coupling of propane to the substrate. We show that both the rate and the nature of the dynamics we measure cannot be reproduced by an existing empirical potential. Using numerical simulation we derive a potential energy surface which is capable of reproducing the main features of our dataset.

[1] Permanent address: Teda Applied Physics School, Nankai University, Tianjin 300457, People's Republic of China.
[2] Author to whom any correspondence should be addressed.

Contents

1. Introduction

Interactions between hydrocarbons and metallic surfaces have been the subject of many experimental and theoretical studies. In part, the motivation for studying these surface systems is related to their important role in industrial catalysis. Advances in theoretical capabilities, which would allow reliable design of new industrial applications [1], rely heavily on the availability of experimental data. Structural measurements, such as the location of the adsorption site, have provided an important benchmark for theoretical developments [2]. A different, particularly sensitive method for studying surface interactions is measuring the dynamics on an atomic scale, as the way the adsorbate moves reflects both the adiabatic interaction with the substrate and the energy transfer rate to and from the surface [3].

A statistical description of motion is given by the pair correlation function, $G(\mathbf{r}, t)$ [4]. This function has a simple classical interpretation, which is the probability of finding a particle at position, $\mathbf{r}$, at a time, t, given that a particle was at the origin at time $t = 0$. The form of this function with t and r, and its dependence on external parameters such as adsorbate coverage and sample temperature, provide insight into the static energy barriers for motion, the frictional coupling of the moving species and the inter-adsorbate interactions [3], [5]–[7].

In practice, measuring $G(\mathbf{r}, t)$ on an atomic length scale is a particularly challenging task. The difficulties arise from the fast timescales on which the characteristic motion takes place. Scanning probe techniques [8], which supply valuable information in real space and real time, are inherently slow. Thus, they can only provide snap shot images of extremely slow jump diffusion, which correspond to either strongly bound systems or ultra cold temperatures. On the other hand, when atomic distances are traveled on a timescale between picoseconds and nanoseconds, quasi-elastic helium atom scattering (QHAS) provides a unique opportunity to measure motion on surfaces [9, 10].

1.1. The experimental technique

The traditional time-of-flight QHAS experiment involves scattering a thermal energy beam of ^{4}He from a surface and measuring the energy of the scattered beam. The apparatus is identical

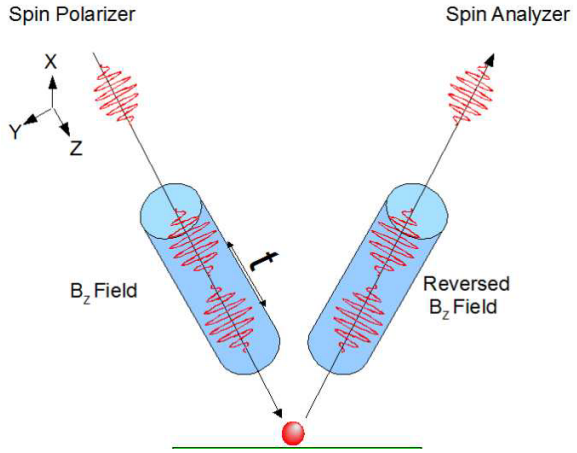

Figure 1. A schematic description of the spin echo principle. The ^{3}He beam is first spin polarized along the y-axis. In a z state representation, the y polarized helium atom can be described as a superposition of two wavepackets with a spin of $\pm\frac{1}{2}$ in the z-direction. The helium beam is then passed through a B_z magnetic field, where the two wavepackets travel at different speeds depending on their spin state, leading to a time difference, t, between the arrival of the two wavepackets to the surface [15]. After scattering from the sample, the effect is reversed using a second magnetic field and the wavepackets are recombined. Motion on the surface causes the two wavepackets to scatter differently, leading to destructive interference of the two wavepackets and a corresponding loss of spin polarization. Thus, the final polarization reflects the motion on the surface during the time, t.

to that used to measure surface vibrations [11]. The dynamic structure factor (DSF), $S(\Delta\mathbf{K}, \omega)$, which is the Fourier transform in time and space of $G(\mathbf{r}, t)$, is deconvoluted from the measured spectrum. The quantity measured in these experiments is the broadening of the elastic peak of the DSF (hence the name quasi-elastic), which is induced by the random motion on the surface.

Due to a fundamental energy resolution limit, the time-of-flight QHAS experiment is restricted to measuring ultra-fast motion [9], which significantly restricted the number of systems that could be studied with this experiment. An alternative technique which circumvents this restriction, is the ^{3}He spin echo technique [12, 13] (^{3}HeSE). This method is a surface sensitive analogue of the neutron spin echo technique [14], and increases the timescale on which QHAS can be used by up to three orders of magnitude. The basic principles of the ^{3}HeSE technique are identical to those of the neutron experiment. The main difference is that the helium experiment is completely surface sensitive as opposed to neutrons which are scattered from within the bulk of the sample.

The principle of the spin echo experiment has been described using various semi-classical and quantum approaches, both for neutrons and for helium beams [10, 15, 16]. The diagram in figure 1 illustrates schematically the basic principle of the technique, following the quantum mechanical description of Gahler *et al* [15]. In a spin echo experiment, the nuclear spin of the beam particles is used to provide the temporal resolution, which is why ^{3}He is used rather than

^{4}He. A magnetic field is used to separate the wavepackets, which correspond to the two spin states of the helium atom, in time and space before scattering from the sample as described in the figure caption. The two wavepackets reach the surface with a relative time difference, t, also known as the spin echo time. A second magnetic field is used to recombine the two wavepackets after scattering. If the surface is static, the wavepackets interfere constructively after the second magnetic field, and the full polarization will be regained. However, if surface motion takes place during the time interval, t, the different scattering events will lead to amplitude and phase differences between the wavepackets and correspondingly a loss of spin polarization. Thus, the final spin polarization, reflects the motion on the surface during the time interval, t.

In a typical ^{3}HeSE experiment, the final spin polarization is measured as a function of the spin echo time, t, and the momentum transfer of the scattering event within the plane of the sample, $\Delta\mathbf{K} = \Delta\mathbf{P}/\hbar$. The time is varied by changing the strength of the magnetic field [15], whereas the momentum transfer, $\Delta\mathbf{K}$, is varied by rotating the sample with respect to the beam line.

Some basic features of the ^{3}HeSE experiment are summarized below:

1. The fastest and slowest motion which can be measured by a ^{3}HeSE experiment are governed by the minimal and maximal achievable separation times between the two wavepackets. In the Cambridge apparatus [17], these times are in the sub picosecond to nanosecond range.
2. The ^{3}HeSE experiment is performed in reciprocal space. Therefore, the smallest length scale of the motion that can be detected is governed by the maximal momentum transfer during scattering. In the Cambridge apparatus [17], momentum transfers of up to ≈ 4 Å $^{-1}$ can be achieved, hence, the technique is sensitive to atomic scale motion.
3. A thermal, low-energy ($<$10 meV), helium beam is typically used. This makes the experiment non-destructive, surface sensitive and chemically inert, allowing the dynamics to be measured in equilibrium with minimal external perturbation.
4. When the energy transfer upon scattering is much smaller than the incident energy, the polarization as a function of $\Delta\mathbf{K}$ and t is proportional to the intermediate scattering function (ISF), $I(\Delta\mathbf{K}, t)$, which is the spatial Fourier transform of the pair correlation function, $G(\mathbf{r}, t)$ and the temporal Fourier transform of the DSF, $S(\Delta\mathbf{K}, \omega)$.[3]
5. For larger energy transfers, a simple procedure, which involves a Fourier transform and a nonlinear transformation, allows us to reconstruct the DSF with an ultra high-energy resolution [10].

2. Experimental details

The experiments were performed with the Cambridge ^{3}HeSE apparatus, the details of which can be found in previous publications [17]. The Pt(111) crystal used in this study was mounted in a UHV chamber with a base pressure of 3×10^{-11} mbar and cleaned by repeated cycling of argon ion sputtering (800 eV, 450 K) and annealing (1100 K).

[3] The direct relation between the scattering experiments and $G(\mathbf{r}, t)$ is obtained using the kinematic single scattering approximation [4, 14]. Previous numerical work justifies this approach, as it shows that the quasi-elastic peak width is not sensitive to the details of the scattering model used [18].

Sub-monolayer propane was adsorbed onto the surface by leaking room temperature propane gas (AirLiquide 99.95% purity) into the UHV chamber. Following the experiment, the temperature programmed desorption spectra was measured while monitoring the specular reflection intensity of the helium beam. A single desorption peak, consistent with previous studies [19], and a simultaneous recovery of the specular helium beam intensity, point to negligible dissociation and contamination at the surface. The measurements presented in this work were performed for a 0.02 ML coverage of propane on the surface (1 ML is defined as an equal number of propane molecules and surface Pt atoms). Propane coverage was estimated by comparing the area under the desorption peak with that of a saturated propane monolayer [20]. Measurements carried out at temperatures higher than 115 K, where desorption occurs, were performed by maintaining an overpressure of propane. The pressure required to maintain the same coverage at different temperatures was calibrated using the specular reflection intensity of the helium beam [21].

3. Propane on Pt(111)—experimental results and basic observations

3.1. The functional form of the polarization curve

Figure 2 shows a typical polarization curve measured as a function of the spin echo time, t. The static contributions to the signal were subtracted from the data[4]. The dominant feature is an exponential decay of the polarization and the red continuous line shows an exponential fit to this decay. This exponential decay corresponds to a sharp Lorentzian quasi-elastic peak (35 μeV FWHM) in the DSF. An exponential decay in time (Lorentzian peak in energy) is expected for a wide variety of diffusion conditions [22]. In particular, such a behavior is expected when either random jump motion or liquid like continuous diffusion dominate the surface dynamics.

Figure 2 shows that in the very first few picoseconds the data deviates from a simple exponential decay. The inset plot shows a polarization measurement, which focuses on the short time range. The deviation is easily seen when comparing the data with the slow exponential decay (red continuous line), which lies clearly beneath it. This deviation from the long timescale behavior is a combination of a fast decay and oscillations. The origin of this weak but complex signal can be understood more readily in the energy domain.

The red markers in figure 3 show the DSF reconstructed[5] from a polarization measurement (figure 2), after subtracting the slow decaying component mentioned above (red line in figure 2). Subtracting this dominant feature enables us to observe the short timescale deviations mentioned above (the green dashed line shows the spectra, divided by 100, without this subtraction).

Two main peaks can be clearly observed above the noise level. The inelastic peak, labeled as 'P' in the plot, located at an energy gain of 5.5 meV. This peak appears with a stronger intensity for a clean platinum surface and its position matches the measured dispersion relation of the Pt(111) surface phonons [23]. The second dominant peak, labeled 'Q_B', is quasi-elastic, i.e. it is centered at a zero energy transfer. It has a FWHM of approximately 1.5 meV, and it

[4] A constant term which corresponds to a static contribution to the signal was subtracted from the polarization. As the static component is also visible on a clean surface, we assigned this contribution to the scattering from the platinum substrate.

[5] The procedure for reconstructing the spectrum requires a complementary measurement of the imaginary component (data not plotted). See [10] for a discussion of this point.

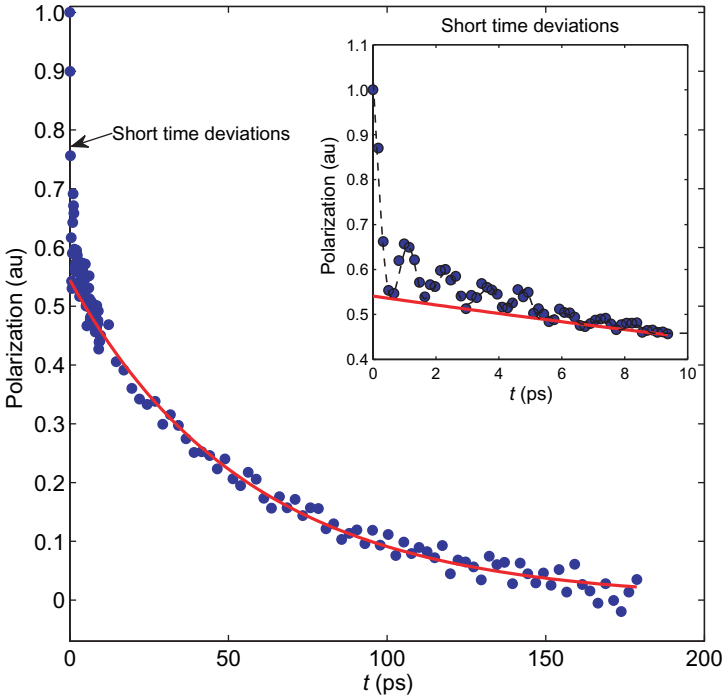

Figure 2. A ^{3}HeSE polarization scan. The circular markers plot the normalized polarization, after subtracting the static contributions to the signal. The scan was measured along the $\langle 1\bar{2}\rangle$ azimuth, at a temperature of 115 K and a momentum transfer of $\Delta K = 0.75\,\text{Å}^{-1}$. The overall decay of the polarization with time is exponential, as demonstrated by the exponential decay fit (continuous red line). A deviation from this behavior can be seen at the very first few picoseconds. The inset plot presents a polarization measurement of these short times. The deviation from the red line, which is the exponential decay seen at longer times is clear and consists of both a fast decay and oscillations.

is only observed after propane adsorption. An additional smaller peak lies in between the two dominant peaks at an energy gain of ≈2.5 meV. The location of this peak suggests that this might be the translational vibrational mode (T-mode) of the propane molecule, however, more measurements with superior signal to noise are needed to confirm the assignment.

In previous helium scattering studies, an estimation of the friction coefficient was derived from the width of the T-mode [24]. In the present study, we chose to extract this information from the broad quasi-elastic peak, which is more intense and can be clearly observed above the noise level. A broad quasi-elastic peak, which underlies an additional, typically much narrower peak (for example the 35 μeV wide peak in figure 3), has been discussed in previous analytical and numerical work [5], [25]–[27]. The broad quasi-elastic peak, along with the energy gain and loss peaks of the T-mode, appears when the surface is sufficiently corrugated, and the adsorbate spends a significant amount of time in the adsorption site. The physical origins of the broad quasi-elastic peak can been related to the frictional coupling of the adsorbate to the substrate, η. Simply speaking, the frictional coupling randomizes the motion within the adsorption site and correspondingly dephases the translational vibration (T-mode), on a $\frac{1}{\eta}$ timescale. In the presence of sufficient frictional coupling, the motion of an adsorbate within the adsorption

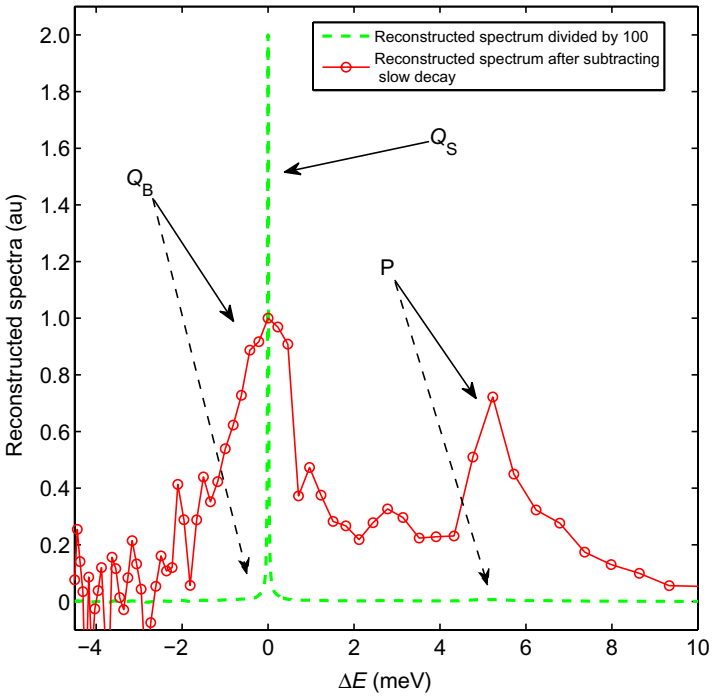

Figure 3. Reconstructing the spectrum of the short time deviations. The red markers show a spectrum reconstructed from the short timescale polarization curve (inset of figure 2), after subtracting the slow exponential decay (red line in figure 2). Two main features, can be clearly seen above the noise: an energy gain peak of $+5.5$ meV (labeled 'P') corresponding to a surface vibration of platinum, and a broad peak centered at $\Delta E = 0$ (labeled 'Q_B'), which arises from the random motion within the adsorption site [5]. The green dashed line shows a spectrum obtained without subtracting the slow decaying exponent (divided by 100). Here, the sharp, 35 μeV FWHM, Lorentzian quasi-elastic peak (labeled 'Q_S'), which corresponds to the slow decay, completely dominates the spectrum, illustrating the importance of subtracting the slow decay in order to study the underlying broad quasi-elastic peak.

site is effectively a combination of random bound diffusion (often called intra-cell diffusion) and vibrations, and gives both quasi-elastic and inelastic peaks, having similar line-width [5]. Extracting the width of the broad quasi-elastic peak, and using the relation between the width of the peak and the friction (equation (2.33) in [27]), we can estimate the friction coefficient for propane to be $\eta = 1.1\ \mathrm{ps}^{-1}$.

3.2. The momentum transfer and temperature dependence of the ISF

Next, we focus on long timescales, and study how the slow decay of the polarization curve changes with the momentum transfer, $\Delta\mathbf{K}$, and the surface temperature. The slow rate of these decays, which correspond to narrow quasi-elastic peaks (FWHM$<100\,\mu$eV), ensure that we are well within the small energy transfer limit we mentioned in section 1.1. Hence, our polarization scans can be directly related to the ISF. All the polarization curves we measured follow simple exponential decays for $t>10$ ps. This allows us to extract the

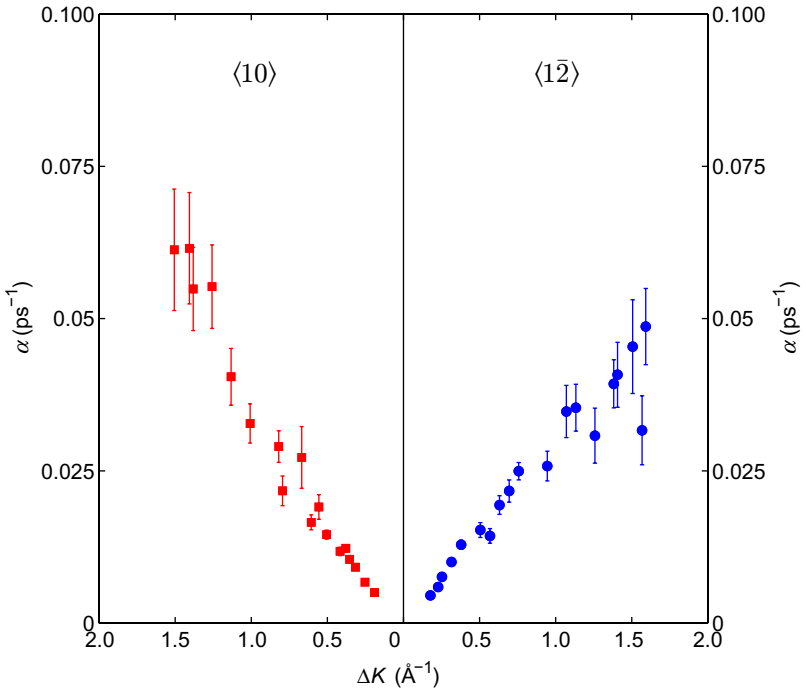

Figure 4. The $\Delta\mathbf{K}$ dependence of the inverse lifetime. The left and right sides of the plot show the inverse lifetimes, extracted from measurements along the $\langle 10 \rangle$ and $\langle 1\bar{2} \rangle$ crystal azimuths, respectively. The measurements were performed at a sample temperature of 115 K. Along both azimuths, α initially increases linearly with $\Delta\mathbf{K}$. Along the $\langle 1\bar{2} \rangle$ azimuth, $\alpha(\Delta\mathbf{K})$ rises less steeply at high $\Delta\mathbf{K}$ values.

inverse lifetime, α, from an exponential fit, $Ae^{-\alpha t}$, to the measurements, and use the $\Delta\mathbf{K}$ and temperature dependence of α to interpret the dynamics. The momentum transfer and temperature dependence of α are plotted in figures 4 and 5, respectively. Some basic properties of the underlying surface dynamics can be extracted directly from these two figures. The key elements are:

1. Figure 4 shows that the inverse lifetimes increase significantly as a function of $\Delta\mathbf{K}$ along both of the azimuths. Such a behavior is expected when the translational motion of the adsorbate dominates the dynamics. The inverse lifetimes we measure cannot be related to a predominant rotational motion, or any other bound motion, as these result in $\Delta\mathbf{K}$ independent inverse lifetimes close to the $\Delta\mathbf{K}$ origin [28].
2. Figure 4 also shows that the inverse lifetimes approach a zero value at $\Delta K = 0$. Thus, the predominant motion of the propane is within the surface plane, and we can rule out the possibility of two different adsorption sites with comparable energies but different heights above the surface [7]. Note that while subtle height difference between adsorption structures, as small as 0.1 Å can be detected with the ^{3}HeSE experiment [7], a height difference at the transition site, where the molecule spends a negligible fraction of the time will not be detected and is not excluded by our results.
3. The initial increase of $\alpha(\Delta\mathbf{K})$ is approximately linear along both the crystal azimuths. This increase clearly deviates both from the quadratic shape expected for liquid-like continuous

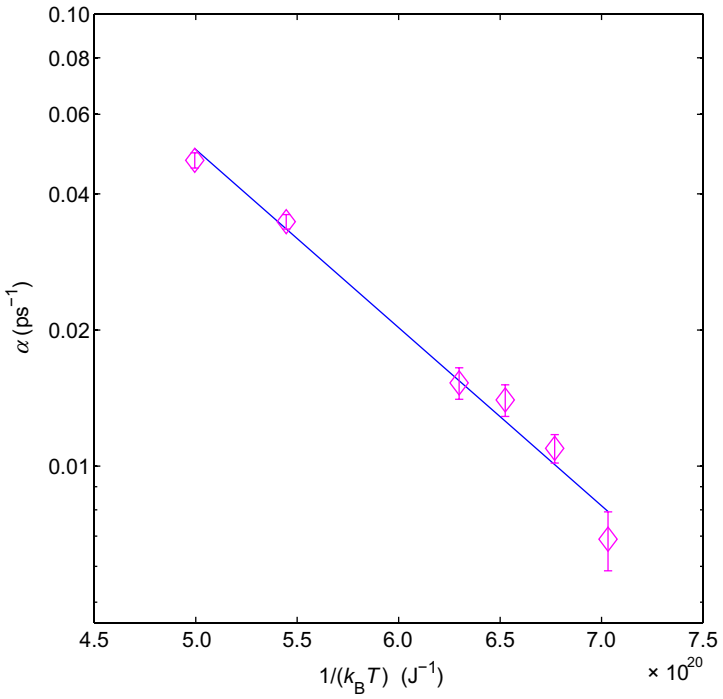

Figure 5. The temperature dependence of the inverse lifetime. The markers plot the inverse lifetimes as function of $1/(k_{\mathrm{B}}T)$, extracted from measurements along the $\langle 1\bar{2}\rangle$ azimuth at $\Delta K = 0.5\,\text{Å}^{-1}$. The blue line shows an Arrhenius fit, which yields an activation energy of 57 ± 4 meV.

diffusion [6, 22] and from the oscillatory dependence of simple single-jump diffusion [29]. A linear $\alpha(\Delta\mathbf{K})$ increase, is consistent with more complex motion such as jump diffusion when a wide distribution of different jump lengths contribute to the surface motion [30][6]. Note that free two-dimensional (2D) gas motion, which also results in a linear $\alpha(\Delta\mathbf{K})$, is not considered as a possibility, as it should produce a Gaussian quasi-elastic peak [31] and correspondingly a Gaussian polarization decay.

4. Figure 5 shows that the inverse lifetimes increase significantly with the surface temperature, and are consistent with thermally activated motion. The Arrhenius fit to the inverse lifetimes measured at $\Delta K = 0.5\,\text{Å}^{-1}$ (continuous line in figure 5), results in an effective energy barrier of 57 ± 4 meV. Thus the corrugation of the potential energy surface (PES), which describes the adiabatic interaction between the propane and the surface, must be of a comparable size[7].

[6] Even in the presence of a wide jump distribution, $\alpha(\Delta\mathbf{K})$ should approach a quadratic behavior at the limit of $\Delta\mathbf{K} \to 0$, however, the experimental $\Delta\mathbf{K}$ range does not include small enough values to show this behavior empirically.

[7] As has been demonstrated numerically [5], the measured activation energy, also known as the effective energy barrier, is frequently lower than the static corrugation value (the height of the PES). This difference is one of the reasons we compare the experiment with molecular dynamics simulation in order to determine the potential rather than using simpler analytical considerations.

4. Propane on Pt(111)—quantitative analysis

4.1. Comparing with an existing interaction model

Ideally, we would use *ab initio* calculations to provide us with an estimate for the propane–platinum interaction. However, we are not currently aware of such studies. The low adsorption energy of propane on platinum and the even smaller energy barriers for diffusion would in fact make such studies particularly challenging at the moment. On the other hand, Stinnett and Madix [32] have developed an empirical model for the interactions between alkanes and the Pt(111) surface.

This empirical model, which we shall refer to as the Stinnett model, was developed to explain the trapping experiments of ethane on a Pt(111) surface [33], and has been shown to successfully predict the trapping properties for other alkanes on Pt(111), including propane [32]. The Stinnett model uses one pairwise Morse potential to describe the interaction between each Pt atom and the methyl or methylene groups of the various alkanes. Thus, propane, which has two methyl groups and one methylene group is represented as a pseudotriatom. The internal degrees of freedom of propane are accounted for using an additional Morse interaction between the methylene–methyl pairs and a bending potential [32]. Finally, it is important to note that in the Stinnett model, the hydrogen atoms are taken into account only through their contribution to the mass of the methyl and methylene groups, respectively, whereas the internal C–H bonds are neglected, as excitations of these modes was considered unlikely at the low temperatures at which propane adsorbs [32].

The validity of a pseudotriatom approach in general, and summation over pairwise interactions in particular, are obviously not guaranteed. However, as this empirical model has been successful in predicting the trapping properties, we have adopted the Stinnett model and its original parameters as a starting point for our analysis. Figure 6 shows the PES, obtained by adding the Stinnett Pt–methyl(methylene) interactions from a three-layer slab of platinum atoms[8]. Note that the PES plotted represents the interaction of each of the methyl or methylene groups with the substrate separately, and is not the overall energy surface for moving the molecule in the plane.

Generally speaking, the PES is a function of the x-, y- and z-coordinates. Figure 6 shows $V_{\text{Stinnett}}(x, y, z_{\text{min}})$, where z_{min} denotes the z value which minimizes the energy at each x, y-coordinate. The location of the maxima and minima lie above the Pt top and hollow sites, respectively. Figure 7 plots $z_{\text{min}}(x, y)$, showing a relatively small variation in the z position of the energy minima, with the highest point located above the top site. Figure 8 shows $V_{\text{Stinnett}}(z)$, calculated above a Pt hollow site.

Plotting the empirical Stinnett PES, and super-imposing a pseudotriatom propane molecule (plotted as three connected circular markers in figure 6), allows us to qualitatively understand the basic dynamics we would expect propane to experience on such a PES. First we note that the corrugation of $V_{\text{Stinnett}}(x, y, z_{\text{min}})$ is small, reaching a maximal value of 30 meV at the Pt surface top site. The almost perfect matching between the geometric structure of propane and the symmetry of the PES, and the small variation in the z_{min} values, allows the two methyls and the methylene to simultaneously lie close to their minimum energy position. The resulting adsorption site for the propane molecule, which approximately occupies three adjacent

[8] The lateral size of each slab was chosen to include contributions from every platinum atom which is within a 9 Å cutoff range [32].

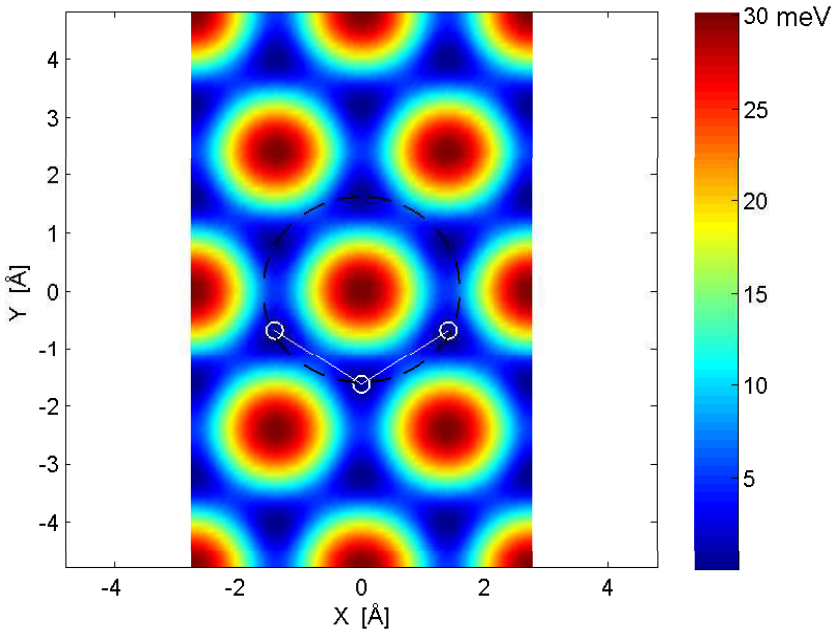

Figure 6. The Stinnett PES. The PES for a methyl/methylene group on Pt(111) calculated from the interaction model suggested by Stinnett and Madix [32]. The color map represents, $V_{\text{Stinnett}}(x, y, z_{\text{min}})$, which is the potential at an x, y-coordinate when the height coordinate, z, is chosen to give the minimal energy. For clarity, a relative energy map is shown, where the lowest energy is given the value of zero, by subtracting the adsorption energy of -147 meV. The white connected circles plot a propane molecule as a pseudotriatom, showing the almost perfect matching between the geometry of the molecule and the minima of the PES at the hollow site. The black dashed circle, is the low energy 'hollow site circle' referred to in the text.

hollow sites, is in agreement with the monolayer structures interpreted from previous LEED data [20].

Next, we can estimate the various energy barriers for the motion of propane from one low-energy site to another. The motion which crosses the lowest energy barrier is a circular rotation of the propane molecule, between the six hollow sites which surround the top site maxima. The black circular line in figure 6 illustrates this low-energy path. A second motion is translation from one of the hollow site circles we just mentioned to a different one (i.e. centered around a different top site). The transition state for this motion involves having one of the methyl groups, or the methylene group fairly close to a top site, hence the energy barrier for this transition is higher than the rotational barrier we discussed, but is still fairly low ($<$30 meV). Finally, we can consider the option of changing the position of one of the methyl groups by performing a 180° flip out of the surface plane. This motion offers another way of moving from one hollow site circle to another. However, as can be seen from figure 8, lifting a methyl unit from the surface increases the energy significantly. In particular, the flip in question involves lifting one of the methyl units by approximately 1.6 Å, which is of the order of 110 meV. Within the temperature range of our measurements (103–145 K), the Boltzmann factor for this motion is smaller by between two and three orders of magnitude with respect to shifting the molecule

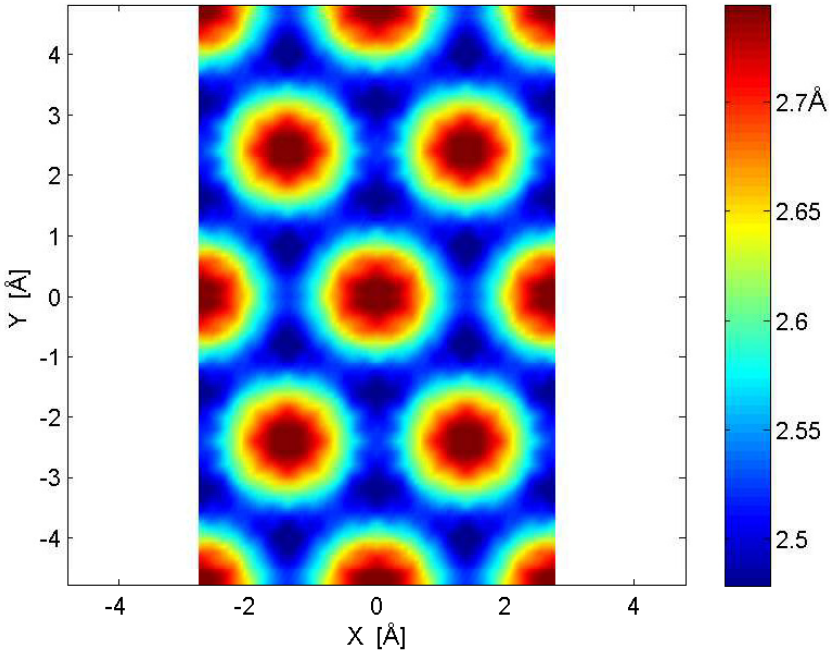

Figure 7. The height of adsorption of the Stinnett interaction. The color plot shows $z_{\min}(x, y)$, which is the z-coordinate that minimizes the Stinnett potential at every x, y point. The $z = 0$ surface was defined as the height of the surface layer Pt ions. The maximum value of $z_{\min}$ is encountered above the top site of the surface.

within the surface plane. Hence, the contribution of a perpendicular flip to the escape rate from a hollow site circle can be safely neglected.

The fact that the energy barriers of the Stinnett potential, for motion within the plane, are significantly lower than the effective energy barrier we measured suggest that this potential is not going to reproduce our measurements. To verify this quantitatively, we use MD simulations, the details of which have been published elsewhere [34]. In these simulations, the trajectories of the moving species are calculated using the Langevin equation, and kinematic scattering calculations are performed in order to simulate the signal and compare with the experiment. The interaction with the substrate atoms is taken into account by two terms. The adiabatic interaction with the surface is described by a PES, whereas the transfer of energy to and from the surface is described by a position-independent friction coefficient, η, and a random impulse term. The strength of the random impulses are determined by a Gaussian distribution, the width of which is related to η through the fluctuation dissipation theorem [35]. Within the coverage range of this study ($\Theta < 0.03$ ML) our results did not show any coverage dependency, therefore we did not include interactions between different propane molecules in the numerical analysis.

For simplicity, the MD simulation was performed using the 2D PES, $V_{\text{Stinnett}}(x, y, z_{\min})$, shown in figure 6, instead of solving the full 3D motion. This simpler treatment was justified on the grounds that the energy barrier for flipping the molecule out of the surface plane makes it an extremely rare event in comparison to motion within the plane. Hence, including the z motion, which introduces an additional vibrational mode, does not alter the in-plane dynamics in any significant way.

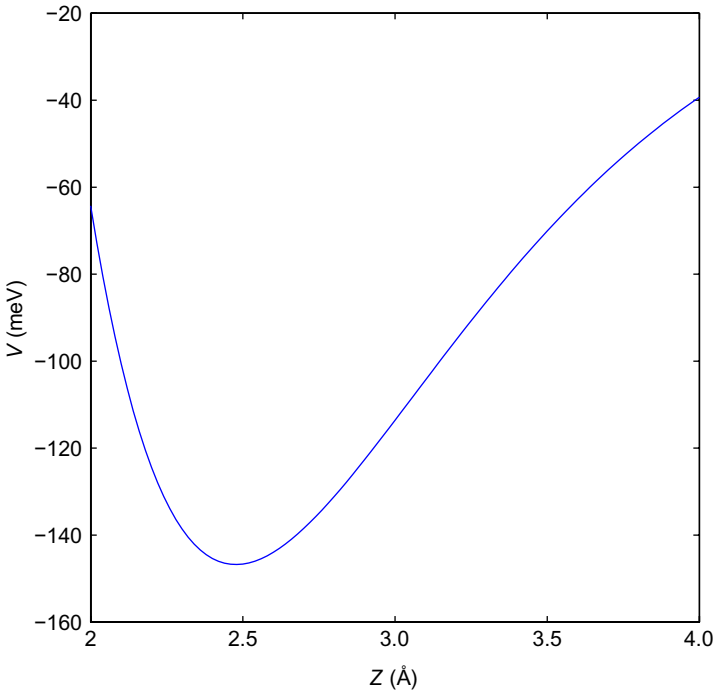

Figure 8. The z dependence of the Stinnett PES. The potential for a methyl/methylene group is plotted as function of the height above the surface. The x, y-coordinates are set above a hollow site, which is the lowest energy site. The $z = 0$ surface was defined as the height of the surface layer Pt ions.

The green solid line in figure 9 shows an ISF calculated by the MD simulation, for the Stinnett PES shown in figure 6, when the sample temperature is 115 K and the scattering calculation is performed for a momentum transfer of, $\Delta K = 0.75\,\text{Å}^{-1}$. The friction coefficient used in the simulation was $\eta = 1.1\,\text{ps}^{-1}$, estimated earlier from the width of the broad quasi-elastic peak (Q_B). One immediate striking feature is the extremely short time on which the ISF decays with respect to the experimental one (figure 2). This reflects a mobility which is significantly higher than the experimentally measured one. In order to assess the impact of our friction estimation on this result, we repeated the simulation using different friction values. The dashed blue line in figure 9 is the result for a substantially lower friction, $\eta = 0.16\,\text{ps}^{-1}$. The resulting mobility is high and in addition the functional form of the polarization deviates from an exponential decay, as expected for sufficiently low friction values [6], in clear contradiction with our experimental data. The dotted red line shows a simulation with a much greater friction value, $\eta = 7\,\text{ps}^{-1}$. At such a high friction value, the motion is slowed down, though still much faster than the experiment. The motion also becomes liquid like and consequently the form of $\alpha(\Delta\mathbf{K})$ is quadratic as shown in the inset plot, contradicting the linearly increasing $\alpha(\Delta\mathbf{K})$ we measure. Finally, for all the friction values we used the effective energy barriers, extracted from Arrhenius fits to the simulation results, are lower than 15 meV. This again is in contrast to the significantly larger activation energy we measure.

Evidently, the low-energy barriers of this PES are responsible for the significantly overestimated mobility. However, simply increasing the corrugation will still not reproduce the observed dynamics, due to the particular geometrical form of the potential. An illustration of

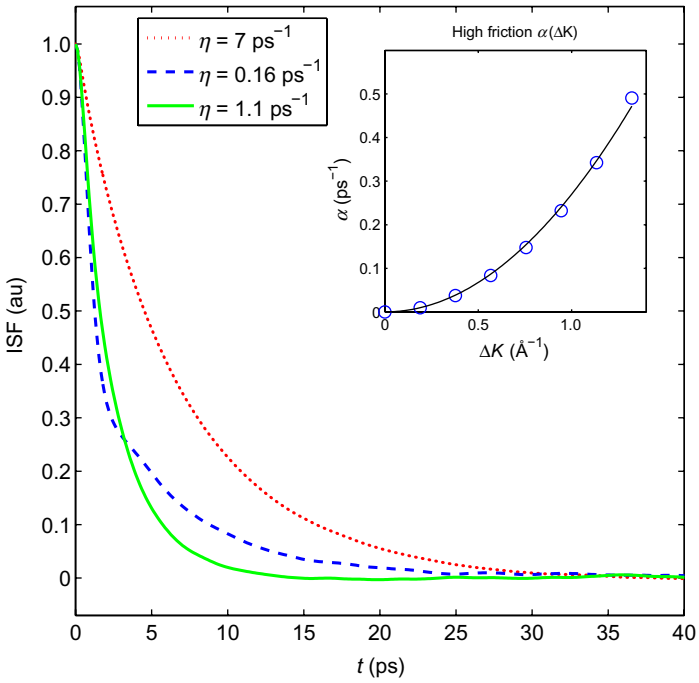

Figure 9. The ISF obtained by MD simulations using the Stinnett PES. The ISF was calculated for $\Delta K = 0.75\,\text{Å}^{-1}$ and $T = 115\,\text{K}$. The blue, green and red lines were calculated for friction values of $\eta = 0.16$, 1.1 and $7\,\text{ps}^{-1}$, respectively. For all of these cases, the decay is faster than that of the experimental measurements. In addition, the low-friction case leads to a non-exponential decay whereas the extremely high-friction case slows down the motion but leads to a liquid-like motion characterized by a quadratic $\alpha(\Delta\mathbf{K})$, again at odds with the experiment. The inset plot shows the $\alpha(\Delta\mathbf{K})$ obtained for the high-friction case, and a quadratic fit to these points (continuous line).

this point can be seen in the simulated ISF shown as a blue solid line in figure 10. This ISF was calculated from a rescaled PES, equal to the Stinnett PES multiplied by a factor of 4. While increasing the corrugation leads to a slower overall decay, the functional form of the decay deviates significantly from a single exponential decay, a fact that is illustrated by the systematic deviations from the single exponential decay fit shown as a red dotted line.

The origin of the deviation from a simple exponential decay can be understood using simple considerations. The polarization curve starts with the typical fast decay and oscillations, which last $\approx 1/\eta$ seconds, and were discussed earlier. This region is marked as τ_{friction} in the figure, and can be seen more clearly in the inset plot. For longer times the decay is characterized by two distinct decay rates, instead of one. This behavior is demonstrated by the dashed green line which is a sum of two exponents, $A_1\exp[-\alpha_1 t] + A_2\exp[-\alpha_2 t]$, which fits the ISF yielding $\alpha_1, \alpha_2 = 0.07, 0.0075\,\text{ps}^{-1}$, respectively. The lifetimes of the two decays $\tau_{1,2} = \frac{1}{\alpha_{1,2}}$ are indicated on the graph to illustrate the two decay rates.

These two very different decay rates correspond to the two distinct motions of the molecule on the surface. The fast component, α_1, corresponds to the fast rotation of the molecule within the hollow site circle we mentioned earlier, the slow component corresponds to the much

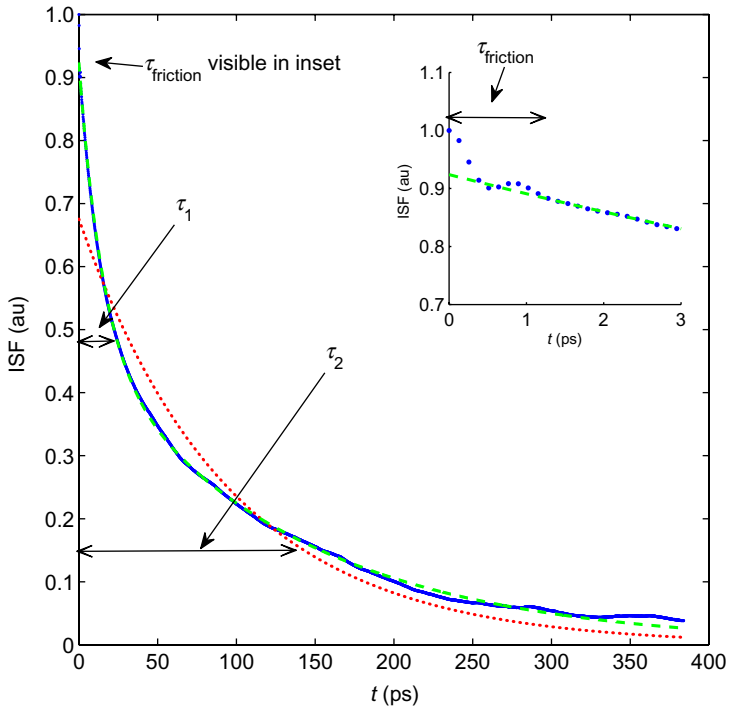

Figure 10. Calculated ISF for a rescaled Stinnett PES. The ISF calculated for a PES which is more corrugated than the Stinnett PES ($\times 4$), at $\Delta K = 1\,\text{Å}^{-1}$, $T = 115\,\text{K}$ and $\eta = 0.8\,\text{ps}^{-1}$. The initial fast decay (marked τ_{friction}), also shown in the inset relates to the intra-cell diffusion described earlier. An attempt to fit the ISF with the functional form of the measurements, i.e. a single exponential decay (red line), illustrated the clear deviation from this functional form. In contrast, the green dashed line is a successful fit to a sum of two exponents, the lifetimes of these two exponents are marked as τ_1 and τ_2 in the figure.

slower rate of escaping from one hollow circle to another[9]. Thus, the much faster rotational motion leads to the deviation from a single exponential decay of the ISF, which is not seen experimentally. Movie 1 (available from stacks.iop.org/NJP/10/125026/mmedia) follows the trajectories of the pseudotriatom, calculated from the same simulation which produced the ISF in figure 10, and illustrates the two different processes graphically.

4.2. Constructing an improved empirical PES

The conclusions obtained from simulating the dynamics on the empirical Stinnett potential and on the rescaled ($\times 4$) version allow us to construct an improved PES that can reproduce the main features of the dynamics seen in the experiment. In particular, the two main properties that we need to modify are: (i) the barriers need to be substantially higher than those of the Stinnett PES, and (ii) the barriers also need to prevent fast rotation within the plane, which leads to a deviation from a single exponential decay behavior.

[9] The assignment of the two different modes was verified using the temperature and $\Delta\mathbf{K}$ dependence of the two components.

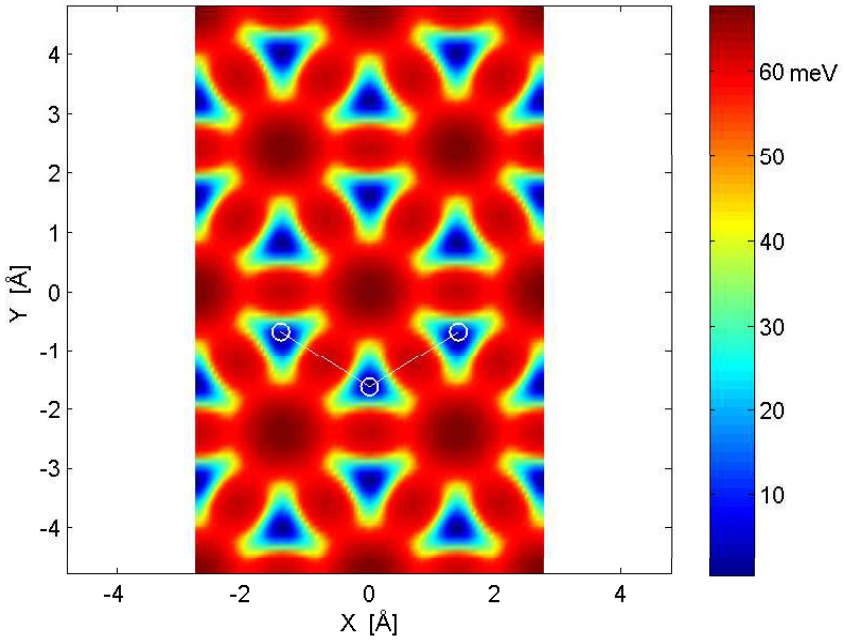

Figure 11. A PES which successfully mimics the measured dynamics. This PES shares the same adsorption geometry as the Stinnett PES, however, additional energy barriers between the hollow sites prevent rotational motion from dominating the dynamics. The white connected circles illustrate propane as a pseudotriatom. The height of the PES corrugation, which is roughly twice as high as the Stinnett PES, was optimized to fit both the temperature and the $\Delta\mathbf{K}$ dependent measurements of the inverse lifetime.

Figure 11 shows a PES which fulfills the requirements above[10]. In addition to being significantly more corrugated than the Stinnett PES, an additional energy barrier is located between the hollow sites, which prevents the rotational motion rate from being faster than the translational motion rate. Within the $\Delta\mathbf{K}$ and temperature range of our experiment, this PES leads to an exponential decaying ISF, which compares well with our experimental results.

The energy barrier height of the PES shown in figure 11, and the friction coefficient were simultaneously optimized to produce the best fit of the simulation to the experiment. The values of this fit are $\eta = 0.8 \pm 0.2\,\mathrm{ps}^{-1}$, in good agreement with our earlier estimation, and a minimal energy barrier for diffusion and rotation of $58 \pm 4\,\mathrm{meV}$. Figures 12 and 13 compare the α values extracted from the measurements and the best fit simulation, for the different $\Delta\mathbf{K}$ and T conditions.

The dynamics calculated with the optimized PES and friction values above reproduce the experimental data very well. A small but significant deviation between the numerical and

[10] The improved empirical PES shown in figure 11 was obtained by modifying the procedure described in [36] in the following way: (i) the sign of the potential was reversed, to obtain hollow site adsorption, and (ii) the corrugation of the potential was made smoother, this was done by performing a square root operation on the values of the potential which are greater than 55 meV. The motivation for choosing a smooth PES, is the fact that regions in the potential which are much higher than the energy barrier to diffusion, reduce the pre-factor for diffusion resulting in motion which is slower than the experimental data.

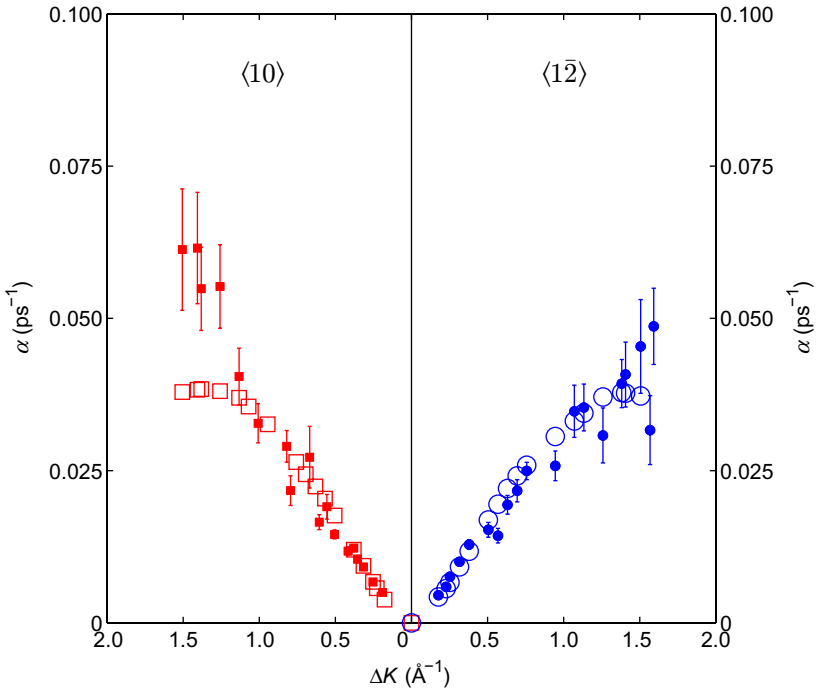

Figure 12. Comparing the $\alpha(\Delta\mathbf{K})$ for the optimized PES and η with the experimental results. The open and full markers show the simulated and experimental $\alpha(\Delta\mathbf{K})$ values, respectively. The results shown on the right and left sides of $\Delta K = 0$, correspond to the $\langle 1\bar{2}\rangle$ and $\langle 10\rangle$ azimuths. While the simulation reproduces most of the experimental results, a deviation which is bigger than the experimental uncertainty can be seen at high $\Delta\mathbf{K}$ values along the $\langle 10\rangle$ crystal azimuth.

experimental results, which seems bigger than the experimental uncertainty, is seen at the very highest $\Delta\mathbf{K}$ points along the $\langle 10\rangle$ azimuth. A difference of $\alpha(\Delta\mathbf{K})$ between the two azimuths, which can be seen in the experimental results, typically reflects a similar difference in the probability for jumping along those two directions [37]. The fact that such an effect is not seen in our simulations suggests that modifying our PES, to make it less isotropic, might improve the quality of the fit at high $\Delta\mathbf{K}$ values. Further measurements at larger values of $\Delta\mathbf{K}$ combined with a study of the propane T-mode, would enable further optimization of the PES, in particular the curvature of the PES at the adsorption site and at the transition sites.

5. Summary and conclusions

^{3}HeSE measurements of propane on a Pt(111) surface have been used to characterize the microscopic surface dynamics of this system. The frictional coupling of propane, within its adsorption site, was estimated as 1.1 ps^{-1} from the width of the broad quasi-elastic peak. The long timescale behavior of the polarization curves, and the way the decay rate varies with $\Delta\mathbf{K}$ and the surface temperature, enables us to deduce that the propane molecule performs translational jump motion, crossing energy barriers which are $\approx$55 meV high.

Using numerical simulations we compared the dynamics to an existing empirical pairwise methyl(methylene)–Pt interaction. The model treats the propane as a pseudotriatom and has

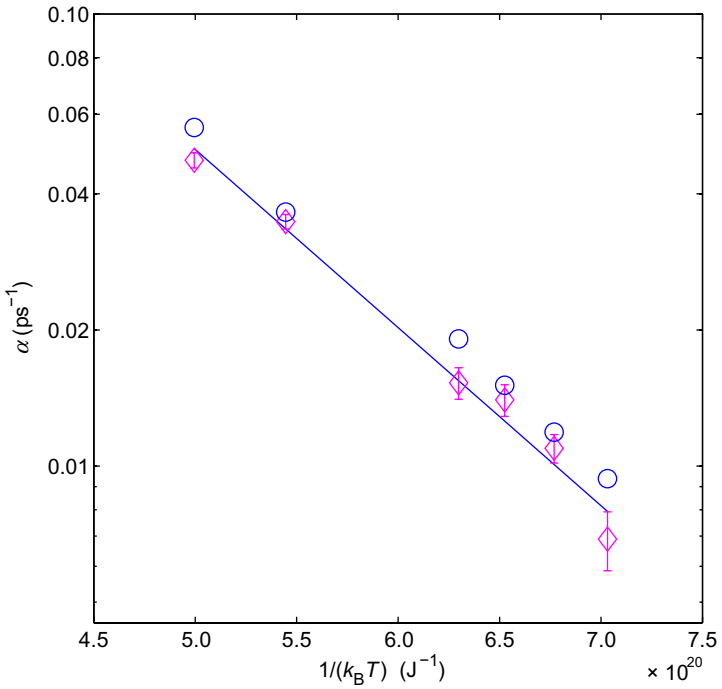

Figure 13. Comparing the Arrhenius plots for the optimized PES and η, with the experimental results. The simulations were performed at the same conditions as the experiment ($\Delta K = 0.5$ Å^{-1} along the $\langle 1\bar{2}\rangle$ azimuth). The experimental points are plotted with diamond markers and the simulated results are plotted as open circles. The line is the same Arrhenius fit shown in figure 5.

been successfully applied to describe the trapping of various alkanes on the Pt(111) surface [32]. Our results show that this empirical model cannot be applied to explain the lateral dynamics of propane on Pt(111), as it predicts a fast translational motion and an even faster rotational motion which can be excluded by our data. The fact that this model successfully describes trapping but fails to describe the dynamics, could be related to the fact that the surface diffusion measurements probe details of the potential around the adsorption configuration, whereas the Stinnett potential has been optimized to fit the trapping experiments which are primarily sensitive to the corrugation of the repulsive region of the potential [32].

We followed the pseudotriatom approach to produce an alternative 2D PES, which can explain all the main properties seen in our results. Optimizing the energy barrier to diffusion and the friction coefficient, this PES reproduces our main results, namely, the functional form of the ISF, the nearly linear increase of the inverse lifetimes as function of $\Delta\mathbf{K}$, their absolute values and their temperature dependence.

The friction coefficient we obtain by fitting our MD simulations to the data is $\eta = 0.8 \pm 0.2\,\mathrm{ps}^{-1}$. The Langevin approach we employ in our simulations [34] assumes that the energy exchange rate is not a function of the spatial coordinates. The fact that the fitted value is in good agreement with our estimation of the friction within the adsorption site suggests that the frictional coupling of propane to Pt(111) does not vary significantly as a function of position.

It is important to emphasize that, while a pseudotriatom PES can reproduce the measured dynamics, our results do not prove that the pseudotriatom approach is in general a valid way of

describing the interaction between the propane and the surface. In particular, it is possible that the interaction of the hydrogens with the surface needs to be explicitly accounted for. However, any alternative more complex PES which is developed using a different approach must still retain the same basic properties as our optimized PES, namely, it must have an energy barrier for both translation and rotation which is approximately 60 meV high.

In summary, our dataset supplies us with an insight into the rate and the nature of the atomic scale motion of propane on Pt(111). The basic dynamical properties we obtained, such as the energy barriers for diffusion and the strength of the frictional coupling, need to be reproduced by any interaction model suggested for this system and therefore supply an important benchmark for future theoretical work.

Acknowledgments

We thank Professor S Miret-Artés for his helpful comments. Instrumental development was supported by a Paul Instrument Fund Grant and the EPSRC. We are grateful for the financial support of Gonville and Caius College, the Royal Society and the EPSRC.

References

[1] Starrost F and Carter E A 2002 *Surf. Sci.* **500** 323
[2] Feibelman P J, Hammer B, Nørskov J K, Wagner F, Scheffler M, Stumpf R, Watwe R and Dumesic J 2001 *J. Phys. Chem.* B **105** 4018
[3] Ala-Nissila T, Ferrando R and Ying S C 2002 *Adv. Phys.* **51** 949
[4] Van Hove L 1954 *Phys. Rev.* **95** 249–62
[5] Jardine A P, Ellis J and Allison W 2004 *J. Chem. Phys.* **120** 8724
[6] Vega J L, Guantes R and Miret-Artés S 2004 *J. Phys.: Condens. Matter* **16** S2879
[7] Alexandrowicz G, Jardine A P, Hedgeland H, Allison W and Ellis J 2006 *Phys. Rev. Lett.* **97** 156103
[8] Binning G, Rohrer H, Gerber Ch and Weibel E 1982 *Phys. Rev. Lett.* **49** 57
[9] Graham A P 2003 *Surf. Sci. Rep.* **49** 115–68
[10] Alexandrowicz G and Jardine A P 2007 *J. Phys.: Condens. Matter* **19** 305001
[11] Hofmann F and Toennies J P 1996 *Chem. Rev.* **96** 1307
[12] Dekieviet M, Dubbers D, Schmidt C, Scholz D and Spinola U 1995 *Phys. Rev. Lett.* **75** 1919–22
[13] Jardine A P, Dworski S, Fouqet P, Alexandrowicz G, Riley D J, Lee G Y H, Ellis J and Allison W 2004 *Science* **304** 1790
[14] Mezei F 1972 *Z. Phys.* **225** 146
[15] Gähler R, Golub R, Habicht K, Keller T and Felber J 1999 *Physica* B **229** 1
[16] Mezei F (ed) 1980 The principles of neutron spin echo *Neutron Spin Echo* (*Lecture Notes in Physics* vol 128) (Berlin: Springer) pp 1–26 doi:10.1007/3-540-10004-0_16
[17] Fouquet P, Jardine A P, Dworski S, Alexandrowicz G, Allison W and Ellis J 2005 *Rev. Sci. Instrum.* **76** 053109
[18] Ellis J, Graham A P, Hofmann F and Toennies J P 2001 *Phys. Rev.* B **63** 195408
[19] Tait S L, Dohnalek Z, Campbell C T and Kay B D 2006 *J. Chem. Phys.* **125** 234308
[20] Carlsson A F and Madix R J 2000 *J. Phys. Chem.* B **105** 12237
[21] Poelsema B, Palmer R L and Comsa G 1984 *Surf. Sci.* **136** 1
[22] Jardine A P, Ellis J and Allison W 2002 *J. Phys.: Condens. Matter* **14** 6173–91
[23] Harten U, Toennies J P, Zhang G and Wöll C 1985 *Phys. Rev. Lett.* **55** 2308
[24] Graham A P and Toennies J P 1998 *Europhys. Lett.* **42** 449
[25] Chen L Y and Ying S C 1993 *Phys. Rev. Lett.* **71** 4361–64
[26] Graham A P, Hofmann F, Toennies J P, Chen L Y and Ying S C 1997 *Phys. Rev.* B **56** 10567–78

[27] Vega J L, Guantes R, Miret-Artés S and Micha D A 2004 *J. Chem. Phys.* **121** 8580
[28] Bee M 1988 *Quasielastic Neutron Scattering* (Bristol: IOP Publishing)
[29] Chudley C T and Elliot R J 1961 *Proc. Phys. Soc. Lond.* **77** 353–61
[30] Ferrando R, Spadacini R and Tommei G E 1993 *Phys. Rev.* E **48** 2437
[31] Ellis J, Graham A P and Toennies J P 1999 *Phys. Rev. Lett.* **82** 5072–5
[32] Stinnett J A and Madix R J 1996 *J. Chem. Phys.* **105** 1609
[33] Stinnett J A, Madix R J and Tully J C 1996 *J. Chem. Phys.* **104** 3134
[34] Ellis J and Graham A P 1997 *Surf. Sci.* **377-379** 833–42
[35] Kubo R 1966 *Rep. Prog. Phys.* **29** 255
[36] Alexandrowicz G, Kole P R, Lee E Y M, Hedgeland H, Ferrando R, Jardine A P, Allison W and Ellis J 2008 *J. Am. Chem. Soc.* **130** 6789–94
[37] Alexandrowicz G, Jardine A P, Fouquet P, Dworski S, Allison W and Ellis J 2004 *Phys. Rev. Lett.* **93** 156103